Article

Molecular Dynamics and Free Energy Simulations of Phenylacetate and CO Release from AMDase and its G74C/C188S Mutant: A Possible Rationale for the Reduced Activity of the Latter

Tarak Karmakar, and Sundaram Balasubramanian

J. Phys. Chem. B, **Just Accepted Manuscript** • DOI: 10.1021/acs.jpcb.6b07034 • Publication Date (Web): 24 Oct 2016

Molecular Dynamics and Free Energy Simulations of Phenylacetate and CO_2 Release from AMDase and its G74C/C188S Mutant: A Possible Rationale for the Reduced Activity of the Latter

Tarak Karmakar and Sundaram Balasubramanian*

Chemistry and Physics of Materials Unit, Jawaharlal Nehru Centre for Advanced Scientific Research, Bangalore 560 064, India, Telephone: +91-80-22082808

E-mail: bala@jncasr.ac.in

*To whom correspondence should be addressed

Abstract

Arylmalonate decarboxylase (AMDase) catalyzes the decarboxylation of α-aryl-α-methyl malonates to produce optically pure α-arylpropionates of industrial and medicinal importance. Herein, atomistic molecular dynamics simulations have been carried out to delineate the mechanism of the release of product molecules, phenylacetate (PAC) and carbon dioxide (CO_2) from the wild-type (WT) and its G74C/C188S mutant enzymes. Both the product molecules follow a crystallographically characterized solvent-accessible channel to come out of the protein interior. A higher free energy barrier for the release of PAC from G74C/C188S compared to that in the WT is consistent with the experimentally observed compromised efficiency of the mutant. The release of CO_2 precedes that of PAC; free energy barriers for CO_2 and PAC release in the WT enzyme are calculated to be $\sim$1-2 kcal/mol and $\sim$23 kcal/mol, respectively. Post-decarboxylation, CO_2 moves toward a hydrophobic pocket formed by Pro 14, Leu 38, Leu 40, Leu 77 and the side chain of Tyr 48 which serves as its temporary 'reservoir'. CO_2 releases following a channel mainly decorated by apolar residues, unlike in the case of oxalate decarboxylase where polar residues mediate its transport.

Introduction

Molecular level investigations of structure and dynamics of an enzyme is of paramount interest to understand its function. In general, the catalytic turnover is constituted by three broad components: substrate binding, catalytic reaction in the active site, and release of products from the protein active site to the exterior.[1,2] Biochemical experiments provide convincing information about the enzyme and its functions, and can throw some light on microscopic details as well. Computer simulations are an excellent complementary tool to reveal details of the system in a dynamical framework. While the substrate (or a small molecule such as a drug) binding[3–7] and the catalytic reaction[8–13] have been studied using molecular modeling methods in a number of enzymes, that of product release has been far and few.[14–21] The current manuscript addresses this issue in a specific decarboxylase enzyme.

Enzymes in the decarboxylase family are vital as they catalyse the decarboxylation of molecules containing mono- and di-carboxylate group in order to produce several chemicals of biological and industrial importance. They also participate in various metabolic pathways in living organisms. Examples of few such decarboxylase enzymes are oxalate decarboxylase,[22,23] acetolactate decarboxylase,[24] arylmalonate decarboxylase[25] etc. In this work, we have performed computational investigations aiming to understand the structure, dynamics and the product release step of arylmalonate decarboxylase (AMDase) using classical molecular dynamics simulations.

AMDase, an enzyme in the decarboxylase family,[26] catalyzes the decarboxylation of aryl-α-malonates to α-arylpropionates and carbon dioxide (CO_2) (Figure S1 of SI).[25] Owing to its metal or cofactor-independent catalytic efficiency (unlike other decarboxylases[27]) and its capability to produce optically pure organic compounds, this enzyme has been claimed to be a promising biocatalyst having biotechnological applications.[13,28–31] Additionally, AMDase has been found to produce several analgesics in the profen groups, e.g., ibuprofen, flurbiprofen, etc.[26,32]

AMDase is a monomeric enzyme with two four-stranded parallel β-sheets, seven promi-

nent α-helices, a few short helices, and random loops. The active site is buried deep inside the protein core (Figure 1), surrounded mostly by α-helices and few random loops.[25] A 'dioxyanion hole' in the reaction center has been proposed to bind two carboxylate groups of the substrate.[25,33,34] While the natural substrate of AMDase is yet to be confirmed, a number of alkenyl- and aryl-malonates are found to get decarboxylated by this enzyme.[33–35] The presence of the aryl (or an alkenyl) group has been proposed to stabilize the enediolate intermediate that is generated during the reaction. Biochemical experiments proposed a two-step decarboxylation mechanism for AMDase,[25] the first being the detachment of one carboxylate group leading to the formation of CO_2 and an enediolate intermediate, followed by the transfer of a proton from an active site residue, Cys 188 to the intermediate so as to produce the monocarboxylate compound. Figure S1 of SI provides the reaction scheme. A recent theoretical study based on quantum chemical cluster calculations has delineated both the mechanism and enantioselectivity of the decarboxylation reaction in AMDase.[13] Biochemical studies have shown that the mutation of Gly 74 (another active site residue) to Cys and Cys 188 to Ser (G74C/C188S) (Figure 1(c)) converted this enzyme to act like a racemase that produces racemic mixtures.[36,37] However, this double mutant showed 20,000 fold lesser activity than the WT enzyme.[38]

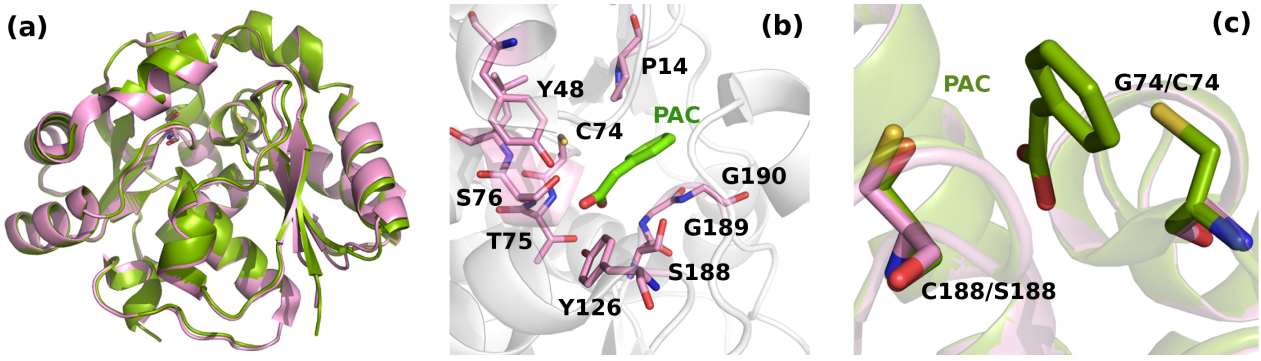

Figure 1: (a) Overlay between the WT (green, PDB ID; 3IP8) and G74C/C188S (pink, PDB ID: 3IXL) mutant enzymes, (b) interactions between phenylacetate (PAC) and residues in the active site of the mutant enzyme, (c) residues in the active site that were mutated.

Okrasa *et al.* have identified a hydrophobic pocket comprising residues P14, L40, Y48, L72, L77 and S76 (Figure 2(a)) to be present near the reaction center which facilitates

the decarboxylation process by destabilizing the carboxylate group in its electrostatically disfavored region.[25] Furthermore, a narrow channel that connects the reaction center to bulk water (Figure 2(b)) has been identified in the crystal structure of AMDase.[25] This solvent-accessible channel has been proposed to be the pathway for the substrate uptake and product release. The phosphate group of benzylphosphate (B85) forms hydrogen bonds with several polar amino acid residues, T75, S76, Y126, and G189. The same residues bind phenylacetate (PAC) in the active site as shown in Figure 1(b) (in the case of the mutant, the crystal structure contains PAC). A π-stack between the phenyl ring of PAC and the amide bond formed between G189 and G190 stabilizes the ligand (substrate and/or product) in the active site (Figure 1(b) and 2(b)). Hydrogen bonding and π-stacking are the two key interactions that mediate the substrate binding in the active site.

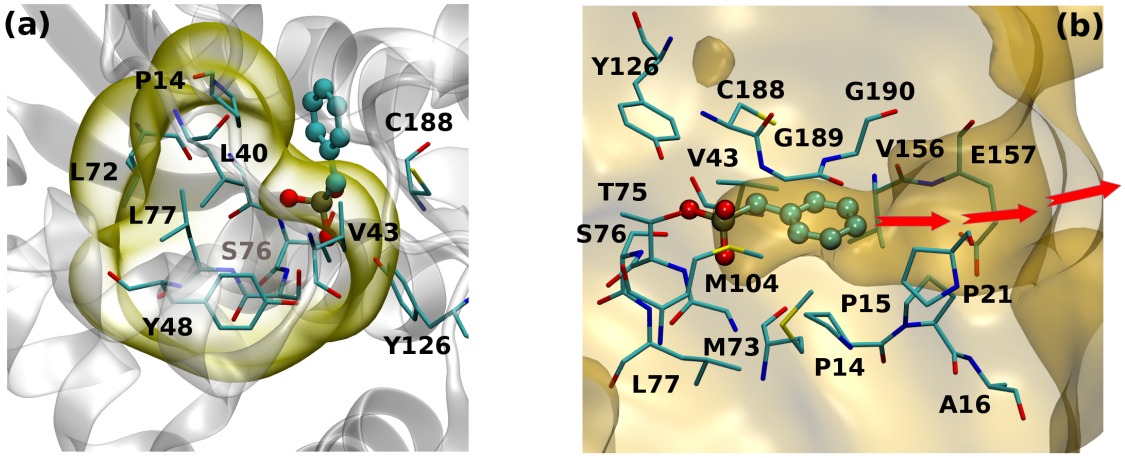

Figure 2: (a) Hydrophobic pocket situated near the reaction center (structure is collected from WT AMDase with PDB ID: 3IP8). The residues forming the hydrophobic pocket are shown both in stick and quicksurf, blown-glass representation as implemented in VMD software.[39] (b) Solvent-accessible channel connecting the active site to bulk water. The residues lining the channel are shown in stick representation.

Although a wealth of information regarding the structure of AMDase and its mutant is available in the literature, a comprehensive molecular level description of the functioning of this important catalyst is yet to be discerned. While the mechanism of the catalytic reaction is known,[13,25] the processes of substrate uptake and product release demand special attention.

Herein, our interest on this enzyme is (i) to study the dynamics of the apo and the products-bound enzymes, (ii) to investigate if the product molecules (PAC and CO_2) release *via* the crystallographically characterized solvent-accessible channel and find out microscopic details of the release pathways, and (iii) to calculate the energetics of the products' escape from the active site of WT and the mutant enzymes to bulk water, and see if it correlates with the reduced catalytic efficiency of the G74C/C188S mutant compared to the WT. Unraveling the product expulsion processes, in turn, would help in gaining knowledge about the mechanism of substrate binding to this enzyme.

In the case of WT AMDase, the catalytic reaction has a rate constant of 260 s^{-1} which can be converted to a free energy barrier of ∼14 kcal/mol.[38] If the product release involves a barrier larger than this value, then it becomes the rate limiting step in the catalytic turnover. An examination of product release is important from this point of view as well.

Investigations on the interactions of small molecules i.e., O_2, CO_2,[40,41] CO,[42,43] NO,[44] and H_2O_2[45] with proteins has been a topic of interest to biochemists.[46] As AMDase produces CO_2 in the catalytic reaction, we were curious to understand the migration of this gas molecule from the active site to bulk water which too has been examined in this work using MD simulations. Results obtained here are compared against our earlier study on oxalate decarboxylase (OXDC).[40] Anticipating our results, we observe a larger free energy barrier for the PAC release in AMDase than what is reported experimentally for the catalytic reaction itself, making the former, the rate limiting step. Further, the calculated product release barrier is higher for the double mutant than that for the WT enzyme, correlating with the reduced activity of the mutant.

Computational methods

Unbiased molecular dynamics (MD) simulations

Initial structures of the WT and the mutant with PDB IDs 3IP8 and 3IXL, respectively were collected from protein data bank (www.rcsb.org). The WT enzyme with PDB ID: 3IP8 contained benzylphosphonate (BP). Retaining the phenyl ring coordinates, the phosphonate group was replaced by an acetate group using GaussView software[47] to generate the initial coordinates for PAC. On the other hand, the mutant enzyme with PDB ID: 3IXL contained PAC itself, and thus the structure was directly used for simulations. Missing residues (residues 1-6 & 239-248 in the case of the WT and residues 1-5 in the case of the mutant) and atoms were added using GaussView software.[47] The generated structures were then protonated and subsequently solvated in water. An appropriate number of counterions (Na^+) were added to neutralize the systems. The systems contained a total number of ∼47,000 to 56,000 atoms. The apo structure of the WT enzyme was obtained by selecting the protein configuration from the last frame (after 500 ps) of the short equilibrium NPT simulation trajectory of PAC-bound WT AMDase, from which the PAC was removed. The resulting pdb was then resolvated. Structural changes which had occurred at the terminii of the collected pdb required more number of water molecules to resolvate it. Details of the systems simulated are presented in Table 1. Minimizations were carried out in two steps, keeping the protein atoms constrained and subsequently, without constraints. The systems were then heated up from 0 to 300 K within 300 ps of NVT simulation, followed by short simulations for 500 ps at 300 K in the NPT ensemble. Nosé-Hoover thermostat[48–50] and Parrinello-Rahman barostat[51] were used to maintain the temperature and pressure at 300 K and 1 bar, respectively. A time step of 1 fs was used to integrate the equations of motion. Covalent bonds involving hydrogen atoms were constrained using LINCS algorithm[52] as implemented in Gromacs simulation package.[53,54] Particle Mesh Ewald method was used to calculate the long-range electrostatic interactions in the systems. Charmm36 force field[55,56]

for the protein and CGenFF parameters[57] for the ligands were used in the simulations. All simulations were carried out in Gromacs-4.5.5 software.[53,54] VMD software[39] was used to visualize the trajectories; both VMD and PyMol[58] were utilized to produce the figures.

Table 1: **Details of the unbiased simulations.**

Systems	Details	No. of atoms	Simulation time (ns)	No. of trajectories	Box length (Å)
WT	Apo	52885	100	1	81.0
	with PAC	47839	100	1	78.3
	with PAC & CO_2	52891	∼10-50	3	81.0
G74C/C188S	Apo	55469	100	1	82.2
	with PAC	55466	100	1	82.3
	with PAC & CO_2	55472	∼10-50	3	82.3

To study the migration of CO_2 in the enzyme and its subsequent release from the protein interior, a CO_2 molecule was placed near the PAC in the initial structures. Once the CO_2 has been placed inside the active site, the structure was minimized using steepest-descent algorithm. The systems were heated from 0 K to 300 K within 300 ps followed by a short simulation of 500 ps in NPT ensemble. Equilibrium simulations aimed at investigating the release of CO_2 were carried out for ∼10-50 ns duration in NPT ensemble at 300 K temperature and 1 bar pressure.

Umbrella Sampling simulations

Additionally, umbrella sampling (US) simulations[59] were performed to calculate the free energy change for the release of CO_2 from AMDase (WT and the mutant). The distance between backbone nitrogen atom of Ser 76 and carbon atom of CO_2 was chosen to be a suitable collective variable (CV) to study the latter's migration. The entire distance (4.5 Å to 15.0 Å) traveled by CO_2 obtained from an unbiased trajectory was divided into small windows of width 0.5 Å. Harmonic umbrella potentials with a force constant of 5 kcal/mol/Å^2 was used in each window to restrict the CO_2 within the reference value of the CV in a window. Each window was then sampled for 500 ps in NVT ensemble to obtain the distribution of the

CV at a particular chosen value. The distribution of last 200 ps of each trajectory was chosen to calculate free energy profiles. The weighted histogram analysis method (WHAM) was used to calculate the PMF of the release process.[60] Such a protocol has been previously followed by Amara *et al.* to study the diffusion of H_2O, O_2 and H_2O_2 in catalase.[45] Multiple independent US simulations (five each for WT and the mutant) with different initial velocity during the sampling of each window were carried out to obtain statistics and confirm the free energy change associated with CO_2 release. Investigations on diffusion of gas molecules in proteins is of long-standing interest in the field of biophysical chemistry. Computer simulations have been performed to understand interaction of gas (and small) molecules with proteins[61,62] and to examine their transport in several such systems.[46,63–68]

Steered MD simulations

Steered molecular dynamics (SMD) is an important tool to investigate ligand binding/unbinding processes in enzymes.[14–20,69,70] SMD simulations were carried out with configurations randomly extracted from the last 20 ns of the unbiased simulation trajectory of the PAC-bound systems. The distance between the centers of mass of Cα of the active site residues, G74 (C74 in the mutant), T75, S76, C188 (S188 in the mutant) and G189, and the heavy atoms of PAC was chosen to be the collective variable (CV). The choice of the CV is based on the observation that these residues are the key ones that bind the PAC in the active site *via* hydrogen bonding. Initially, a few SMD simulations were carried out to optimize the force constant of the spring and the pulling velocity. Use of lower force constant (10 or 20 kcal/mol/Å^2) of the spring was found to disobey the stiff-spring approximation which is the heart of SMD simulation. On the other hand, a very very slow pulling velocity (0.25 Å/ns) required long sampling time, and the trajectory was not found to follow stiff-spring approximation. Thus, a higher force constant and relatively faster pulling velocity were used in the SMD simulations. Three sets of SMD simulations each for WT and the mutant with pulling velocities of 1 Å/ns, 0.75 Å/ns, and 0.5 Å/ns and a force constant of 50 kcal/mol/Å^2

were performed. Fifteen trajectories were generated with each of the pulling velocities (see Table 2). Potential of mean forces (PMF) were calculated from the work profiles of each set obtained from the SMD simulations using Jarzynski's equality.[71,72] All SMD simulations were carried out in Gromacs software patched with Plumed-1.3 plugin.[73]

Table 2: **Details of the systems and the SMD simulations of PAC bound AMDase**

Systems	**Pulling velocity** (Å/ns)	**Simulation time** time (ns)	**No. of trajectories**
WT	0.5	30	15
	0.75	20	15
	1.0	15	15
G74C/C188S	0.5	30	15
	0.75	20	15
	1.0	15	15

Results

The stability of the apo and the ligand-bound enzymes are confirmed by plotting the RMSDs of their backbone atoms as a function of equilibrium simulation time, shown in Figure S2 of SI. The RMSD fluctuations of Cα atoms of WT and the mutant assure significant stability of both the systems and reveal no significant difference (Figure S2 of SI) indicating that the mutation does not affect the overall dynamics of the enzyme. Additionally, the presence of the ligand molecule in the active site does not provide any extra stability to the enzymes.

Side chains of T75, S76 and Y126, and backbone -NH of G74 and G189 form hydrogen bonds with the carboxylate group of PAC and thereby stabilize it in the active site. The phenyl ring of PAC forms a π-stack with the amide bond formed between G189 and G190.[25] This interaction is very important in two ways: firstly, the π-stack helps in binding the aryl group of the substrate in the active site and secondly, it stabilizes the negative charge that arises on the enediolate intermediate during the catalytic reaction. In the unbiased simulations of the PAC bound enzyme (both WT and the mutant), the π-stack remains

stable over the entire simulation time span (Figure S3 of SI).

PAC release from WT and the mutant

In all unbiased simulations of the PAC-bound systems, PAC does not move away from its binding zone due to strong hydrogen bonding interactions between its carboxylate group and the polar active site residues, T75, S76, and Y126. Therefore, we accelerated the release of PAC by drawing it away from the active site using steered molecular dynamics (SMD) simulations.[70] An examination of all the SMD trajectories reveals that PAC follows the solvent-accessible channel to egress of the enzyme (Figure 3(a)). Work profiles obtained

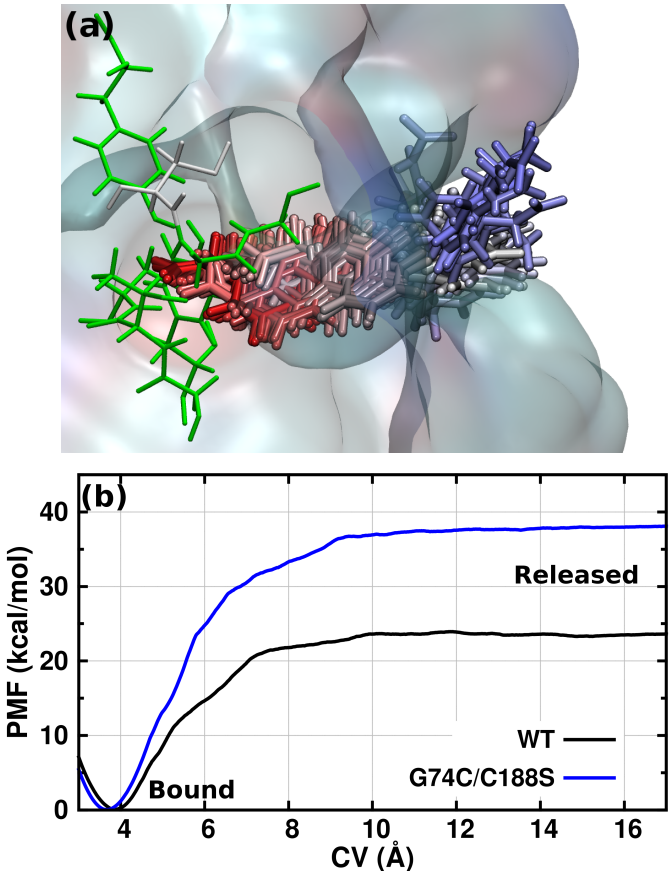

Figure 3: (a) Release of PAC from the active site of the WT enzyme. Instantaneous positions of PAC are shown in stick representation, red and blue colors indicate the initial and final positions of the molecule. (b) averaged PMF profile for the release of PAC from the active site of WT (black) and the mutant (blue) enzymes.

from each set are provided in Figures S4 and S5 of SI. The PMF profiles (individual profiles

are shown in Figure S6 of SI) obtained from the three sets (each for WT and the mutant) are averaged, and are provided in Figure 3(b). Free energy barriers of ∼23 kcal/mol and ∼37 kcal/mol were obtained for the release of PAC from the WT enzyme and the mutant, respectively (Figure 3(b)). A considerably higher free energy barrier for the release of PAC from the mutant compared to that in the WT system could be related to the compromised activity of the former as observed in biochemical investigations.[38] Zhang *et al.* obtained a free energy change of ∼21 kcal/mol for the unbinding of an acetamidomethylene substrate (containing two carboxylate groups) from a hydrolase.[74] In another study, the binding of allophanate (with one carboxylate group) in allophanate hydrolase was found to involve a free energy change of ∼17 kcal/mol.[75] Thus, the value of ∼23 kcal/mol for the WT AMDase reported here is in line with these earlier investigations concerning the binding/unbinding of mono- or di-carboxylate substrates in enzymes.

Mechanism of PAC release

We next examine the mechanism of the escape of PAC and the residues that mediate its expulsion. PAC resembles an amphiphile, having a charged carboxylate at one end and a hydrophobic phenyl ring on the other. During its release from the active site, at first, the interactions between the carboxylate group of the ligand and the residues (G74, S76, T75, Y126, and C188) binding it get disrupted (Figure 4(i, ii)). Simultaneously, the π-stack between the phenyl ring of PAC and the amide bond formed by G189 and G190 is ruptured (Figure 4(iii, iv)). These two processes are the main contributors for the crossing of a high free energy barrier as manifested in the regions of 8-9 Å of the PMF plots (Figure 3(b)). The presence of additional hydrogen bonding interactions exerted by the side chains of C74 and S188 in the mutant enzyme increases the free energy barrier, relative to WT (Figure S7 of SI). An opening of the gate (residues 39-45 and 151-161, forming two flexible loops, Figure S8 of SI) has been observed during the release of the PAC from both the systems (Figure S9 of SI). The closure of the active site upon substrate binding by these flexible loops has

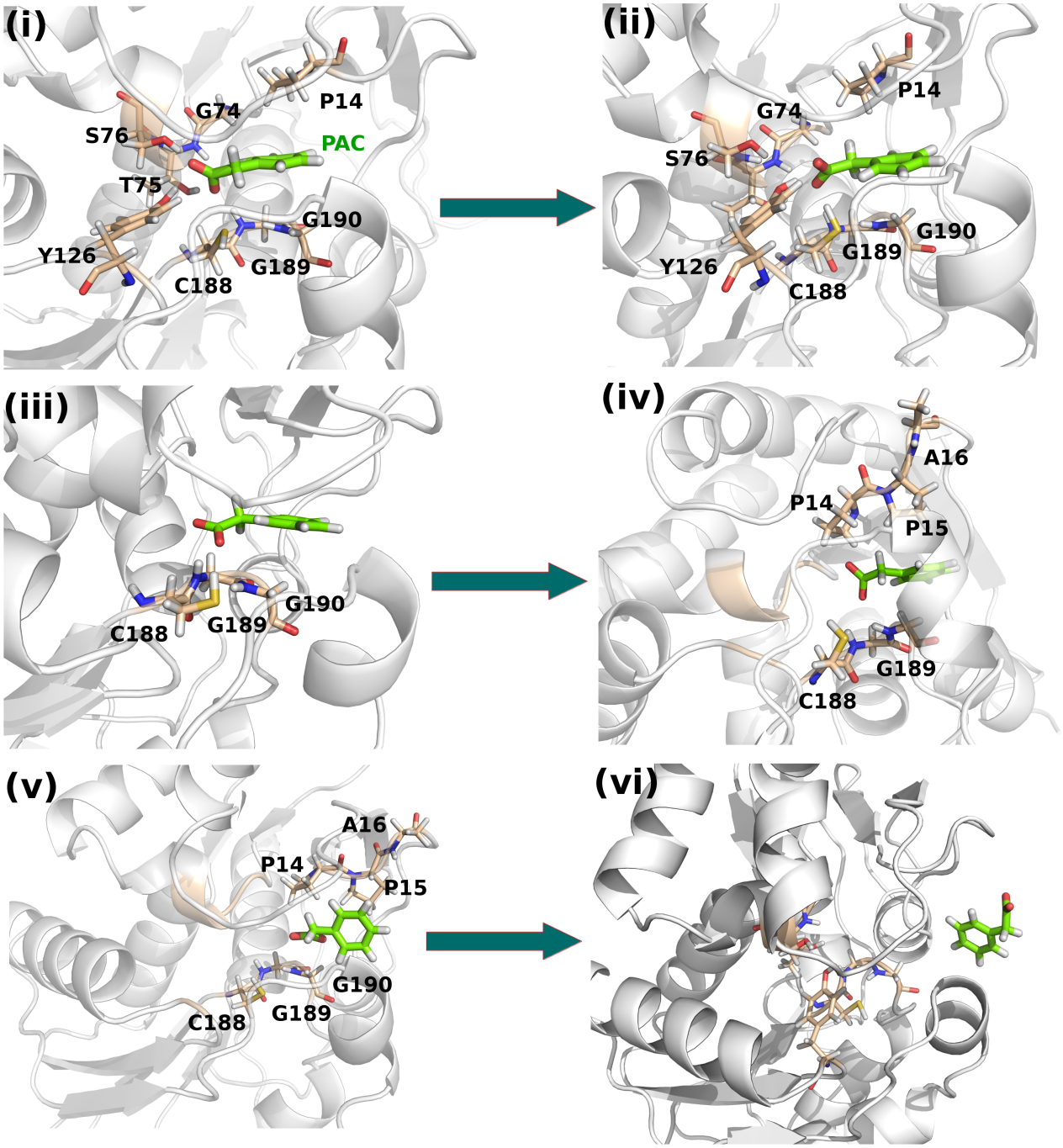

Figure 4: Detailed steps of the PAC release from the WT enzyme; configurations are chosen from a single SMD trajectory. (i) Initial PAC-bound state, residues binding the PAC are shown in wheat colored sticks, (ii) twisting of PAC (this corresponds to the minimum at CV=4 Å in the PMF profiles) (iii) sliding of the π-stack between the phenyl ring of PAC and amide bond between G189 and G190, (iv) disruption of the π-stack and further movement of PAC toward the mouth of the channel, (v) PAC at the entrance of the channel, and (vi) final release of PAC from the enzyme.

previously been proposed for this enzyme.[33] Once the interactions between the active site residues are lost, PAC moves further away from its binding site toward the entrance of the channel (Figure 4(v)) and finally gets released (Figure 4(vi)). Hydrophobic residues such as V156, A16, P14, P15, and L19 present at the entrance of the channel (inside the circle) interact with the phenyl group of PAC (Figure 5).

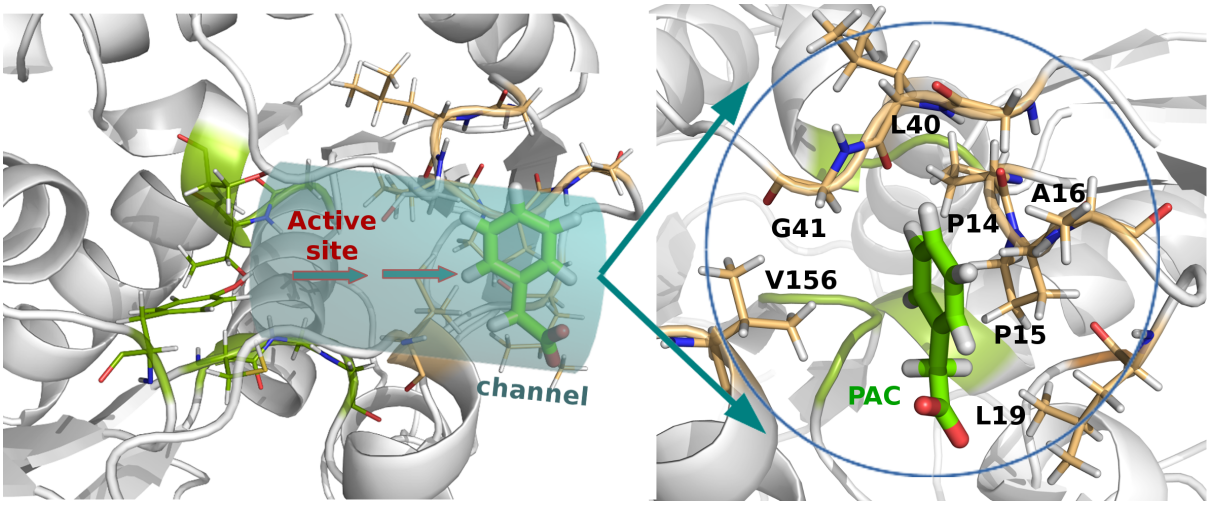

Figure 5: Interactions of PAC with the hydrophobic residues present at the entrance of the channel. Active site residues are shown in green color, and the channel in cyan colored cylinder. The residues interacting with PAC at the mouth (circle) of the channel are shown in stick representation (wheat color).

CO_2 Release

To study the motion of CO_2 inside the pocket and its subsequent release, additional simulations in which a CO_2 molecule was placed near the PAC were carried out. It can be surmised that CO_2 should initially be located near the PAC where one of its carboxylate groups must have detached during the catalytic reaction (Figure 6(a)). The PAC-CO_2 bound systems were simulated (equilibrium) for ∼10-50 ns at 300 K temperature in the NPT ensemble. Multiple, independent trajectories (three each for WT and the mutant) of PAC-CO_2 systems have been generated to confirm the release pathway (Figure 6(b)) for CO_2. Unlike PAC, CO_2 was found to get released spontaneously in equilibrium simulations, and thus

SMD runs were not warranted. The movement of the CO_2 molecule from the active site to bulk water was examined by the time evolution of the distance between nitrogen atom of S76 residue and the carbon atom of CO_2 (Figure 6(c) and (d) and Figure S10 of SI). The release of CO_2 takes place within ∼10-40 ns of simulation time.

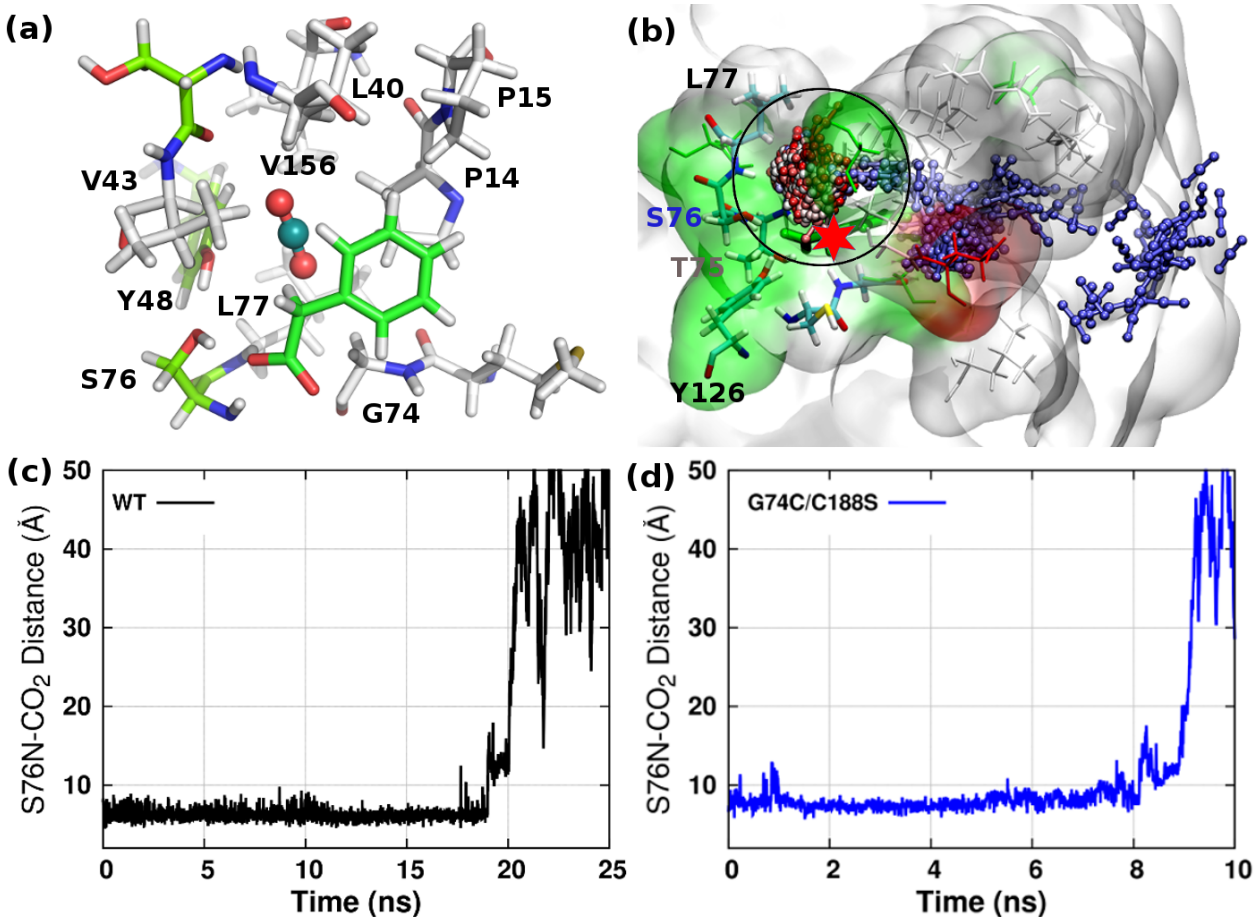

Figure 6: (a) Residence of CO_2 in the hydrophobic pocket, (b) release of CO_2 from the active site of WT AMDase to bulk water; location of CO_2 inside the hydrophobic pocket is depicted by a circle; residues lining the CO_2 migration path are shown in stick representation, white: hydrophobic residues and green & red: polar residues. The figure represents CO_2 migration data from an equilibrium simulation trajectory (WT) of length 25 ns. Equally spaced, five thousand frames were extracted from the trajectory. Out of them, the positions of CO_2 in only 4050 frames are shown here for clarity. The release of CO_2 from the left (active site, situated near red asterisk) to the right (bulk water) can be seen. The change in color of CO_2 molecules from red to blue via white indicates initial, intermediate, and final locations of the molecule in the channel. Distance between nitrogen of S76 located near the active site and carbon of CO_2, is plotted as a function of unbiased simulation time for (c) WT and (d) mutant enzymes from one trajectory. Results from other trajectories are provided in Figure S10 of SI.

Hydrophobic pocket - a temporary 'reservoir' for CO_2

In the simulation trajectories of the PAC-CO_2 systems, the CO_2 molecule transits toward the hydrophobic pocket, which serves as its temporary '*reservoir*' (Figure 6(b) circled). Once CO_2 leaves this pocket, it follows the solvent-accessible channel to escape the enzyme (shown in Figure 6(b)). The amino acids lining this channel are identified by calculating the distances between any atom of CO_2 and the atoms in residues with which it is interacting. A cut-off distance of 3 Å was used in this exercise. The calculated distances were then sorted to obtain the minimum distance between CO_2 and any residue in the path of its transportation. The list of residues interacting with CO_2 thus obtained is displayed in Table 3. Details of the individual contacts are provided in Table S1 of SI.

Table 3: CO_2 interacts with the amino acids listed here during its release via the solvent accessible channel in WT enzyme.

Amino Acids	Pro	Val	Tyr	Leu	Ser	Gly	Ala	Met	Glu
Residue no.	14	13	48	19	42	74	22	73	157
	15	43		40	76	190	25	159	
	21	156		77	212		160		
				192					

Umbrella sampling simulations provide the energetics of the release of CO_2 from the enzyme interior to bulk water. A representative plot demonstrating the overlapping of the distribution of the CV at different windows is shown in Figure S11 of SI. Individual PMF profiles (five each for WT and the mutant) for the release of CO_2 from WT and the mutant enzymes are provided in the SI (Figure S12). The PMF profiles obtained from all US simulations were averaged to obtain an averaged PMF plot, shown in Figure 7(a) and (b). The release of CO_2 from the active site to the bulk water is found to involve a free energy barrier of ∼1-2 kcal/mol with a minimum near 6 Å for the WT (Figure 7(a)) and ∼7.5 Å for the mutant (Figure 7(b)). This region corresponds to the hydrophobic pocket, and the free energy minimum at this zone further confirms the temporary residence of the gas

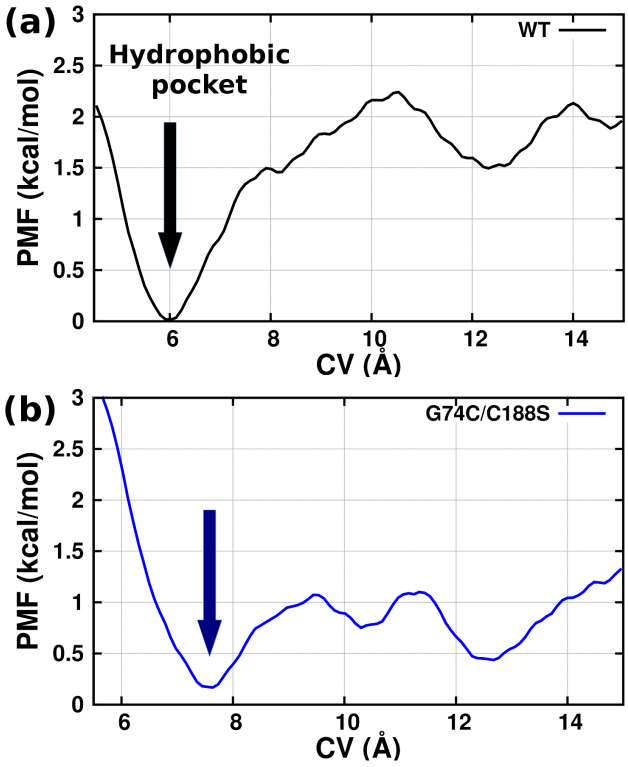

Figure 7: PMF profiles for the release of CO_2 from (a) WT and (b) the mutant enzymes, respectively. The hydrophobic pocket where CO_2 stays *prior* to its release is shown by an arrow in both the systems.

molecule in the pocket. The free energy minimum in the mutant is shallower than in WT, and its position is shifted toward right (Figure 7(b)). This is due to the presence of C74 occupying the pocket which does not allow the CO_2 to reside in the pocket and permits CO_2 to get released in a more facile manner that in WT. The low values of free energy barrier for CO_2 release allowed us to observe its escape within a few nanoseconds even in the unbiased simulation trajectories. The free energy difference between the CO_2 bound to the active site of the WT enzyme and that in bulk solution is $\sim$2.0 kcal/mol, while it is around 1.0 kcal/mol in the mutant. Monte-Carlo bootstrapping analysis (as implemented in the WHAM code) was carried out to calculate the errors in the free energy. An average error of $\pm$0.02 kcal/mol has been obtained. A representative PMF plot with the error bars is provided in Figure S13 of SI.

Discussion

Transport of a substrate from bulk water to the buried active site, and conversely, the release of the products following similar or different channels are two key events in an enzymatic turnover. The facile release of CO_2 from the PAC-CO_2 bound systems within a few nanoseconds of simulation time reveals that CO_2 indeed is likely to be the first candidate to escape the enzyme, followed by the release of PAC. While the release of CO_2 is associated with a very low free energy barrier (of ∼1-2 kcal/mol), that for PAC is ∼23 kcal/mol in WT AMDase. Osterman *et al.* reported an initial fast release of CO_2, a 'burst phase', in another enzyme of decarboxylase family, ornithine decarboxylase (ODC).[76] The release of CO_2 within a few nanoseconds of unbiased simulations was also observed in our earlier investigation on oxalate decarboxylase (OXDC)[40] suggesting that CO_2 release could be facile among decarboxylases.

In WT ornithine decarboxylase (ODC), the release of the second product, putrescine has been reported to be the rate limiting step,[27,76] with a rate of dissociation (k_{-2}) of 0.0035 s^{-1}, corresponding to a free energy barrier of ∼21 kcal/mol (using Transition State Theory).[76] Given the approximations in computational modeling and differences between the enzymes, the value of ∼23 kcal/mol obtained by us for WT AMDase here is not too different for the experimentally determined free energy barrier for product release in WT ODC. On this note, an experimental determination of the rate of dissociation of the PAC from AMDase would help in confirming our results related to the energetics of the product release. The reduced efficiency of the mutant compared to that of the WT enzyme could be due to the higher free energy barrier for the release of PAC from the former than the latter. However, it should be realized that the overall reduced efficiency of the AMDase mutant relative to the WT enzyme may not be solely dependent on the less favorable product release in the former; other factors including substrate binding and the rate of the catalytic reaction itself could influence the activity. However, as stated before, we have focussed here on the product release step alone.

Due to the high free energy barrier, the release of PAC is likely to be the rate limiting

step. In the case of WT AMDase, the catalytic reaction has a rate constant (k_{cat}) of 260 s^{-1} [38] which can be converted to a free energy barrier (using Transition State Theory) of ~14 kcal/mol. In the case of G74C/C188S, the rate constant is 0.020 s^{-1} corresponding to a free energy barrier of ~20 kcal/mol.[38] Our simulations provide a free energy barrier of ~23 kcal/mol and ~37 kcal/mol for the release of PAC from WT and the mutant, respectively. Based on these data, we propose that the product release could be the slowest step of the catalytic turnover and thus, the rate limiting step of this enzyme. However, further experimental investigations are required to confirm our results.

Our investigations on products' release from AMDase provided two important outcomes, the first being the identification of a hydrophobic pocket for the temporary residence of CO_2. The pocket's function is two-fold; it facilitates the decarboxylation of malonate by exerting a hydrophobic pull (engineering this pocket by mutating few residues led to a 9,500 fold improved catalytic efficiency[77]) on one of the carboxylate groups, as investigated by Yoshida *et al.*[77] and later, acting as a temporary 'reservoir' for the generated CO_2 molecule. We have previously observed the existence of a similar pocket for the residence of CO_2 in OXDC.[40] It remains to be seen if such a hydrophobic pocket is a common feature in all decarboxylases. The second outcome from our study is that, unlike in OXDC where the release of CO_2 from the active site to bulk water takes place via a polar channel comprising of polar amino acids, e.g., Asp, Glu, Arg and His,[40] in AMDase, CO_2 follows a channel that is decorated mostly by hydrophobic residues (Table S1 of SI). It would be interesting to investigate different types (based on the chemical nature of the residues) of channels (in both globular enzymes and membrane proteins) through which the migration of CO_2 takes place. On this note, van Lun *et al.* have shown that CO_2 prefers hydrophobic residues[41] while previous investigations[40,62] of enzyme-CO_2 systems have delineated the role of polar residues like Arg, Tyr and His in binding CO_2 in enzyme cavities. Further studies in this field are required to draw general conclusions about the behavior of CO_2 in enzymes that either sequester CO_2 or produce it.

The release of PAC from the active site of AMDase to bulk water along the solvent-

accessible channel is mediated by interactions with several residues lining it. The hydrophobic residues present at the entrance of the channel modulate the final escape of PAC. It is thus not unlikely to visualize their participation in the recognition of alkenyl and aryl malonate substrates during the substrate binding step as well. A plausible mechanism for the substrate binding would be, an initial recognition of alkenyl or aryl group of a substrate by the hydrophobic entrance, followed by the formation of a π-stack between the side chain of the substrate with the amide bond between G189 and G190. In the final step, polar residues Ser 76, Thr 75, Tyr 126 and Cys 188 present in the active site drag two carboxylate groups of the substrate and thereby bind the substrate. *Thus, a mechanism of hydrophobic 'pull' for the release of PAC and a 'push' for the binding of the substrate toward the active site can be prescribed for this enzyme.*

Conclusions

In summary, based on extensive simulations, this work provides the following outcomes: (i) the reduced efficiency of the G74C/C188S mutant reported in experiments could have contributions from the higher free energy barrier for the release of second product molecule (PAC) in the mutant as compared to that in the WT enzyme, and (ii) a hydrophobic recognition mechanism may be operative for the binding of the substrate, thereby modulating their specificity in AMDase, (iii) release of CO_2 precedes the expulsion of PAC, the latter could be the rate limiting step of the enzyme, (iv) temporary residence of CO_2 in the hydrophobic 'reservoir' and (v) CO_2 migrates *via* a channel mostly decorated by apolar amino acids residues unlike in OXDC where polar residues mediate its transport from the active site to bulk water.

Supporting Information

The Supporting Information contains figures reaction scheme, RMSD plots, work profiles, PMF profiles for the release of PAC from WT and mutant, formation of hydrogen bonds between PAC and active site residues in the mutant enzyme, gate formed between two loops & gate width plots, CO_2 release profiles, a table listing residues lining the CO_2 migration channel, CV distribution plot obtained from US simulation, individual PMF profiles obtained from US simulations for the release of CO_2 from WT and the mutant enzymes, and a PMF plot with free energy error bars.

Acknowledgement

T. K. and S. B. thank the Department of Science and Technology, India for support. T. K. acknowledges UGC for senior research fellowship.

References

(1) Segel, I. H. *Enzyme kinetics*; Wiley, New York, 1975; Vol. 957.

(2) Garcia-Viloca, M.; Gao, J.; Karplus, M.; Truhlar, D. G. How Enzymes Work: Analysis by Modern Rate Theory and Computer Simulations. *Science* **2004**, *303*, 186–195.

(3) Goodsell, D. S.; Olson, A. J. Automated Docking of Substrates to Proteins by Simulated Annealing. *Proteins: Struct. Funct. Bioinf.* **1990**, *8*, 195–202.

(4) Kua, J.; Zhang, Y.; McCammon, J. A. Studying Enzyme Binding Specificity in Acetylcholinesterase Using a Combined Molecular Dynamics and Multiple Docking Approach. *J. Am. Chem. Soc.* **2002**, *124*, 8260–8267.

(5) Okazaki, K.-i.; Takada, S. Dynamic Energy Landscape View of Coupled Binding and

Protein Conformational Change: Induced-Fit Versus Population-Shift Mechanisms. *Proc. Natl. Acad. Sci.* **2008**, *105*, 11182–11187.

(6) Tao, Y.; Rao, Z.-H.; Liu, S.-Q. Insight Derived from Molecular Dynamics Simulation into Substrate-Induced Changes in Protein Motions of Proteinase K. *J. Biomol. Struct. Dyn.* **2010**, *28*, 143–157.

(7) Buch, I.; Giorgino, T.; De Fabritiis, G. Complete Reconstruction of an Enzyme-Inhibitor Binding Process by Molecular Dynamics Simulations. *Proc. Natl. Acad. Sci.* **2011**, *108*, 10184–10189.

(8) Warshel, A. Computer Simulations of Enzyme Catalysis: Methods, Progress, and Insights. *Annu. Rev. Biophys. Biomol. Struct.* **2003**, *32*, 425–443.

(9) Friesner, R. A.; Guallar, V. Ab Initio Quantum Chemical and Mixed Quantum Mechanics/Molecular Mechanics (QM/MM) Methods for Studying Enzymatic Catalysis. *Annu. Rev. Phys. Chem.* **2005**, *56*, 389–427.

(10) Senn, H. M.; Thiel, W. QM/MM Studies of Enzymes. *Curr. Opin. Chem. Biol.* **2007**, *11*, 182–187.

(11) Stanton, C. L.; Kuo, I.-F. W.; Mundy, C. J.; Laino, T.; Houk, K. N. QM/MM Metadynamics Study of the Direct Decarboxylation Mechanism for Orotidine-5'-Monophosphate Decarboxylase Using Two Different QM Regions: Acceleration too Small to Explain Rate of Enzyme Catalysis. *J. Phys. Chem. B* **2007**, *111*, 12573–12581.

(12) Hou, Q.; Gao, J.; Liu, Y.; Liu, C. A QM/MM Study on the Catalytic Mechanism of Pyruvate Decarboxylase. *Theor. Chem. Acc.* **2012**, *131*, 1–9.

(13) Lind, M. E.; Himo, F. Theoretical Study of Reaction Mechanism and Stereoselectivity of Arylmalonate Decarboxylase. *ACS Catal.* **2014**, *4*, 4153–4160.

(14) Martínez, L.; Webb, P.; Polikarpov, I.; Skaf, M. S. Molecular Dynamics Simulations of Ligand Dissociation from Thyroid Hormone Receptors: Evidence of the Likeliest Escape Pathway and its Implications for the Design of Novel Ligands. *J. Med. Chem.* **2006**, *49*, 23–26.

(15) Liu, X.; Xu, Y.; Wang, X.; Barrantes, F. J.; Jiang, H. Unbinding of Nicotine from the Acetylcholine Binding Protein: Steered Molecular Dynamics Simulations. *J. Phys. Chem. B* **2008**, *112*, 4087–4093.

(16) Klvana, M.; Pavlova, M.; Koudelakova, T.; Chaloupkova, R.; Dvorak, P.; Prokop, Z.; Stsiapanava, A.; Kuty, M.; Kuta-Smatanova, I.; Dohnalek, J. Pathways and Mechanisms for Product Release in the Engineered Haloalkane Dehalogenases Explored using Classical and Random Acceleration Molecular Dynamics Simulations. *J. Mol. Biol.* **2009**, *392*, 1339–1356.

(17) Li, W.; Shen, J.; Liu, G.; Tang, Y.; Hoshino, T. Exploring Coumarin Egress Channels in Human Cytochrome P450 2A6 by Random Acceleration and Steered Molecular Dynamics Simulations. *Proteins: Struct. Funct. Bioinf.* **2011**, *79*, 271–281.

(18) Kalyaanamoorthy, S.; Chen, Y.-P. P. Exploring Inhibitor Release Pathways in Histone Deacetylases Using Random Acceleration Molecular Dynamics Simulations. *J. Chem. Inf. Model.* **2012**, *52*, 589–603.

(19) Shen, Z.; Cheng, F.; Xu, Y.; Fu, J.; Xiao, W.; Shen, J.; Liu, G.; Li, W.; Tang, Y. Investigation of Indazole Unbinding Pathways in CYP2E1 by Molecular Dynamics Simulations. *PloS one* **2012**, *7*, e33500.

(20) Biedermannová, L.; Prokop, Z.; Gora, A.; Chovancová, E.; Kovács, M.; Damborskỳ, J.; Wade, R. C. A Single Mutation in a Tunnel to the Active Site Changes the Mechanism and Kinetics of Product Release in Haloalkane Dehalogenase LinB. *J. Biol. Chem.* **2012**, *287*, 29062–29074.

(21) Karmakar, T.; Roy, S.; Balaram, H.; Prakash, M. K.; Balasubramanian, S. Product Release Pathways in Human and Plasmodium falciparum Phosphoribosyltransferase. *J. Chem. Inf. Model.* **2016**, *56*, 1528–1538.

(22) Anand, R.; Dorrestein, P. C.; Kinsland, C.; Begley, T. P.; Ealick, S. E. Structure of Oxalate Decarboxylase from Bacillus subtilis at 1.75 Å Resolution. *Biochemistry* **2002**, *41*, 7659–7669.

(23) Just, V. J.; Stevenson, C. E.; Bowater, L.; Tanner, A.; Lawson, D. M.; Bornemann, S. A Closed Conformation of Bacillus subtilis Oxalate Decarboxylase OxdC Provides Evidence for the True Identity of the Active Site. *J. Biol. Chem.* **2004**, *279*, 19867–19874.

(24) Marlow, V. A.; Rea, D.; Najmudin, S.; Wills, M.; Fulop, V. Structure and Mechanism of Acetolactate Decarboxylase. *ACS Chem. Biol.* **2013**, *8*, 2339–2344.

(25) Okrasa, K.; Levy, C.; Hauer, B.; Baudendistel, N.; Leys, D.; Micklefield, J. Structure and Mechanism of an Unusual Malonate Decarboxylase and Related Racemases. *Chem. Eur. J.* **2008**, *14*, 6609–6613.

(26) Kourist, R.; Guterl, J.-K.; Miyamoto, K.; Sieber, V. Enzymatic Decarboxylationan Emerging Reaction for Chemicals Production from Renewable Resources. *ChemCatChem* **2014**, *6*, 689–701.

(27) Brooks, H. B.; Phillips, M. A. Characterization of the Reaction Mechanism for Trypanosoma brucei Ornithine Decarboxylase by Multiwavelength Stopped-Flow Spectroscopy. *Biochemistry* **1997**, *36*, 15147–15155.

(28) Matoishi, K.; Ueda, M.; Miyamoto, K.; Ohta, H. Mechanism of Asymmetric Decarboxylation of α-Aryl-α-Methylmalonate Catalyzed by Arylmalonate Decarboxylase Originated from Alcaligenes bronchisepticus. *J. Mol. Catal. B: Enzym* **2004**, *27*, 161–168.

(29) Terao, Y.; Ijima, Y.; Miyamoto, K.; Ohta, H. Inversion of Enantioselectivity of Arylmalonate Decarboxylase via Site-Directed Mutation Based on the Proposed Reaction Mechanism. *J. Mol. Catal. B: Enzym* **2007**, *45*, 15–20.

(30) Miyamoto, K.; Tsutsumi, T.; Terao, Y.; Ohta, H. Stereochemistry of Decarboxylation of Arylmalonate Catalyzed by Mutant Enzymes. *Chem. Lett.* **2007**, *36*, 656–657.

(31) Tamura, K.; Terao, Y.; Miyamoto, K.; Ohta, H. Asymmetric Decarboxylation of α-Hydroxy- and α-Amino-α-Phenylmalonate Catalyzed by Arylmalonate Decarboxylase from Alcaligenes bronchisepticus. *Biocatal. Biotransfor.* **2008**, *26*, 253–257.

(32) Gaßmeyer, S. K.; Wetzig, J.; Mügge, C.; Assmann, M.; Enoki, J.; Hilterhaus, L.; Zuhse, R.; Miyamoto, K.; Liese, A.; Kourist, R. Arylmalonate Decarboxylase-Catalyzed Asymmetric Synthesis of Both Enantiomers of Optically Pure Flurbiprofen. *ChemCatChem* **2016**, *8*, 916–921.

(33) Kuettner, E. B.; Keim, A.; Kircher, M.; Rosmus, S.; Strter, N. Active-Site Mobility Revealed by the Crystal Structure of Arylmalonate Decarboxylase from Bordetella bronchiseptica. *J. Mol. Biol.* **2008**, *377*, 386 – 394.

(34) Okrasa, K.; Levy, C.; Wilding, M.; Goodall, M.; Baudendistel, N.; Hauer, B.; Leys, D.; Micklefield, J. Structure-Guided Directed Evolution of Alkenyl and Arylmalonate Decarboxylases. *Angew. Chem. Int. Ed.* **2009**, *48*, 7691–7694.

(35) Miyamoto, K.; Ohta, H. Enzyme-Mediated Asymmetric Decarboxylation of Disubstituted Malonic Acids. *J. Am. Chem. Soc.* **1990**, *112*, 4077–4078.

(36) Terao, Y.; Miyamoto, K.; Ohta, H. Introduction of Single Mutation Changes Arylmalonate Decarboxylase to Racemase. *Chem. Commun.* **2006**, 3600–3602.

(37) Obata, R.; Nakasako, M. Structural Basis for Inverting the Enantioselectivity of Arylmalonate Decarboxylase Revealed by the Structural Analysis of the

Gly74Cys/Cys188Ser Mutant in the Liganded Form. *Biochemistry* **2010**, *49*, 1963–1969.

(38) Miyauchi, Y.; Kourist, R.; Uemura, D.; Miyamoto, K. Dramatically Improved Catalytic Activity of an Artificial (S)-selective Arylmalonate Decarboxylase by Structure-Guided Directed Evolution. *Chem. Commun.* **2011**, *47*, 7503–7505.

(39) Humphrey, W.; Dalke, A.; Schulten, K. VMD: Visual Molecular Dynamics. *J. Mol. Graphics* **1996**, *14*, 33–38.

(40) Karmakar, T.; Periyasamy, G.; Balasubramanian, S. CO2 Migration Pathways in Oxalate Decarboxylase and Clues about its Active Site. *J. Phys. Chem. B* **2013**, *117*, 12451–12460.

(41) van Lun, M.; Hub, J. S.; van der Spoel, D.; Andersson, I. CO2 and O2 Distribution in Rubisco Suggests the Small Subunit Functions as a CO2 Reservoir. *J. Am. Chem. Soc.* **2014**, *136*, 3165–3171.

(42) Ruscio, J. Z.; Kumar, D.; Shukla, M.; Prisant, M. G.; Murali, T.; Onufriev, A. V. Atomic Level Computational Identification of Ligand Migration Pathways between Solvent and Binding Site in Myoglobin. *Proc. Natl. Acad. Sci. USA* **2008**, *105*, 9204–9209.

(43) Bossa, C.; Anselmi, M.; Roccatano, D.; Amadei, A.; Vallone, B.; Brunori, M.; Di Nola, A. Extended Molecular Dynamics Simulation of the Carbon Monoxide Migration in Sperm Whale Myoglobin. *Biophysical J.* **2004**, *86*, 3855–3862.

(44) Mishra, S.; Meuwly, M. Nitric Oxide Dynamics in Truncated Hemoglobin: Docking Sites, Migration Pathways, and Vibrational Spectroscopy from Molecular Dynamics Simulations. *Biophysical J.* **2009**, *96*, 2105–2118.

(45) Amara, P.; Andreoletti, P.; Jouve, H. M.; Field, M. J. Ligand Diffusion in the Catalase

from Proteus mirabilis: A Molecular Dynamics Study. *Protein Sci.* **2001**, *10*, 1927–1935.

(46) Cohen, J.; Arkhipov, A.; Braun, R.; Schulten, K. Imaging the Migration Pathways for O2, CO, NO, and Xe Inside Myoglobin. *Biophysical J.* **2006**, *91*, 1844–1857.

(47) Dennington, R.; Keith, T.; Millam, J. GaussView, Version 5.0. 9, Shawnee Mission Semichem. *Inc.,, KS* **2009**,

(48) Nosé, S. A Unified Formulation of the Constant Temperature Molecular Dynamics Methods. *J. Chem. Phys.* **1984**, *81*, 511–519.

(49) Nosé, S. A Molecular Dynamics Method for Simulations in the Canonical Ensemble. *Mol. Phys.* **1984**, *52*, 255–268.

(50) Hoover, W. G. Canonical Dynamics: Equilibrium Phase-Space Distributions. *Physical Rev. A* **1985**, *31*, 1695.

(51) Parrinello, M.; Rahman, A. Polymorphic Transitions in Single Crystals: A New Molecular Dynamics Method. *J. Appl. Phys.* **1981**, *52*, 7182–7190.

(52) Hess, B.; Bekker, H.; Berendsen, H. J.; Fraaije, J. G. LINCS: A Linear Constraint Solver for Molecular Simulations. *J. Comput. Chem.* **1997**, *18*, 1463–1472.

(53) Hess, B.; Kutzner, C.; Van Der Spoel, D.; Lindahl, E. GROMACS 4: Algorithms for Highly Efficient, Load-Balanced, and Scalable Molecular Simulation. *J. Chem. Theory Comput.* **2008**, *4*, 435–447.

(54) Pronk, S.; Páll, S.; Schulz, R.; Larsson, P.; Bjelkmar, P.; Apostolov, R.; Shirts, M. R.; Smith, J. C.; Kasson, P. M.; van der Spoel, D. GROMACS 4.5: A High-Throughput and Highly Parallel Open Source Molecular Simulation Toolkit. *Bioinformatics* **2013**, btt055.

(55) Cornell, W. D.; Cieplak, P.; Bayly, C. I.; Gould, I. R.; Merz, K. M.; Ferguson, D. M.; Spellmeyer, D. C.; Fox, T.; Caldwell, J. W.; Kollman, P. A. A Second Generation Force Field for the Simulation of Proteins, Nucleic Acids, and Organic Molecules. *J. Am. Chem. Soc.* **1995**, *117*, 5179–5197.

(56) Bjelkmar, P.; Larsson, P.; Cuendet, M. A.; Hess, B.; Lindahl, E. Implementation of the CHARMM Force Field in GROMACS: Analysis of Protein Stability Effects from Correction Maps, Virtual Interaction Sites, and Water Models. *J. Chem. Theory Comput.* **2010**, *6*, 459–466.

(57) Vanommeslaeghe, K.; Hatcher, E.; Acharya, C.; Kundu, S.; Zhong, S.; Shim, J.; Darian, E.; Guvench, O.; Lopes, P.; Vorobyov, I. CHARMM General Force Field: A Force Field for Drug-Like Molecules Compatible with the CHARMM All-Atom Additive Biological Force Fields. *J. Comput. Chem.* **2010**, *31*, 671–690.

(58) Schrödinger, L. The PyMOL Molecular Graphics System, Version 1.3 r1. *Py-MOL, The PyMOL Molecular Graphics System, Version* **2010**, *1*.

(59) Torrie, G. M.; Valleau, J. P. Nonphysical Sampling Distributions in Monte Carlo Free-Energy Estimation: Umbrella Sampling. *J. Comput. Phys.* **1977**, *23*, 187–199.

(60) Kumar, S.; Rosenberg, J. M.; Bouzida, D.; Swendsen, R. H.; Kollman, P. A. The Weighted Histogram Analysis Method for Free-Energy Calculations on Biomolecules. I. The Method. *J. Comput. Chem.* **1992**, *13*, 1011–1021.

(61) Cundari, T. R.; Wilson, A. K.; Drummond, M. L.; Gonzalez, H. E.; Jorgensen, K. R.; Payne, S.; Braunfeld, J.; De Jesus, M.; Johnson, V. M. CO2-Formatics: How Do Proteins Bind Carbon Dioxide? *J. Chem. Inf. Model.* **2009**, *49*, 2111–2115.

(62) Drummond, M. L.; Wilson, A. K.; Cundari, T. R. Carbon Dioxide Migration Pathways in Proteins. *J. Phys. Chem. Lett.* **2012**, *3*, 830–833.

(63) Kottalam, J.; Case, D. A. Dynamics of Ligand Escape from the Heme Pocket of Myoglobin. *J. Am. Chem. Soc.* **1988**, *110*, 7690–7697.

(64) Fiorucci, S.; Golebiowski, J.; Cabrol-Bass, D.; Antonczak, S. Molecular Simulations Reveal a New Entry Site in Quercetin 2, 3-Dioxygenase. A Pathway for Dioxygen? *Proteins: Struct. Funct. Bioinf.* **2006**, *64*, 845–850.

(65) Maragliano, L.; Cottone, G.; Ciccotti, G.; Vanden-Eijnden, E. Mapping the Network of Pathways of CO Diffusion in Myoglobin. *J. Am. Chem. Soc.* **2009**, *132*, 1010–1017.

(66) Wang, X. S.; Roitberg, A. E.; Richards, N. G. Computational Studies of Ammonia Channel Function in Glutamine 5-Phosphoribosylpyrophosphate Amidotransferase. *Biochemistry* **2009**, *48*, 12272–12282.

(67) Wang, S.; Orabi, E. A.; Baday, S.; Berneche, S.; Lamoureux, G. Ammonium Transporters Achieve Charge Transfer by Fragmenting their Substrate. *J. Am. Chem. Soc.* **2012**, *134*, 10419–10427.

(68) Baday, S.; Orabi, E. A.; Wang, S.; Lamoureux, G.; Bernèche, S. Mechanism of NH4+ Recruitment and NH3 Transport in Rh Proteins. *Structure* **2015**, *23*, 1550–1557.

(69) Lüdemann, S. K.; Lounnas, V.; Wade, R. C. How do Substrates Enter and Products Exit the Buried Active Site of Cytochrome P450cam? 1. Random Expulsion Molecular Dynamics Investigation of Ligand Access Channels and Mechanisms. *J. Mol. Biol.* **2000**, *303*, 797–811.

(70) Park, S.; Schulten, K. Calculating Potentials of Mean Force from Steered Molecular Dynamics Simulations. *J. Chem. Phys.* **2004**, *120*, 5946–5961.

(71) Jarzynski, C. Nonequilibrium Equality for Free Energy Differences. *Phys. Rev. Lett.* **1997**, *78*, 2690.

(72) Jarzynski, C. Equilibrium Free-Energy Differences from Nonequilibrium Measurements: A Master-Equation Approach. *Phys. Rev. E* **1997**, *56*, 5018.

(73) Bonomi, M.; Branduardi, D.; Bussi, G.; Camilloni, C.; Provasi, D.; Raiteri, P.; Donadio, D.; Marinelli, F.; Pietrucci, F.; Broglia, R. A. PLUMED: A Portable Plugin for Free-Energy Calculations with Molecular Dynamics. *Comp. Phys. Comm.* **2009**, *180*, 1961–1972.

(74) Zhang, J.-L.; Zheng, Q.-C.; Li, Z.-Q.; Zhang, H.-X. How Does (E)-2-(Acetamidomethylene) Succinate Bind to its Hydrolase? From the Binding Process to the Final Result. *PloS one* **2013**, *8*, e53811.

(75) Zhang, Z.; Zhang, J.; Zheng, Q.; Kong, C.; Li, Z.; Zhang, H.; Ma, J. Theoretical Investigation on Binding Process of Allophanate to Allophanate Hydrolase. *Chem. Res. Chinese U.* **2015**, *31*, 1023–1028.

(76) Osterman, A. L.; Brooks, H. B.; Jackson, L.; Abbott, J. J.; Phillips, M. A. Lysine-69 Plays a Key Role in Catalysis by Ornithine Decarboxylase through Acceleration of the Schiff Base Formation, Decarboxylation, and Product Release Steps. *Biochemistry* **1999**, *38*, 11814–11826.

(77) Yoshida, S.; Enoki, J.; Kourist, R.; Miyamoto, K. Engineered Hydrophobic Pocket of (S)-Selective Arylmalonate Decarboxylase Variant by Simultaneous Saturation Mutagenesis to Improve Catalytic Performance. *Biosci. Biotechnol. Biochem.* **2015**, *79*, 1965–1971.

Table of Contents